Journal of Power Sources, 45 (1993) 93–103

A novel Pd–Ag membrane anode for alkaline fuel cells suitable for CO_2-containing hydrogen

Ph. Hasler and Th. Allmendinger*

Swiss Federal Institute of Technology, Department of Chemical Engineering and Industrial Chemistry, 8092 Zurich (Switzerland)

(Received April 6, 1992; in revised form December 24, 1992; accepted January 5, 1993)

Abstract

A novel type of a selectively hydrogen-permeable membrane is presented. The membrane consists of a poreless Pd–Ag film with a thickness of about 1 μm on a nickel-sieve structure serving as a porous support material. A palladinated and additionally platinated membrane has been tested as a hydrogen anode in 10 M KOH in the range of 55 and 106 °C. It has been found that the anodic current density is limited by the kinetics of gas-side surface reactions of hydrogen and/or by the hindered transition at the interfaces between the catalytic palladium layers and the Pd–Ag film. On the electrolyte side, the surface diffusion on the additionally deposited platinum turned out to be important. At an overpotential of 100 mV and at 120 °C, a current density of about 0.5 A/cm^2 has been estimated for pure hydrogen and normal pressure.

Introduction

Alkaline fuel cells exhibit some advantages over acidic fuel cells due to less severe corrosion problems, generally lower material costs and higher system efficiency. However, the incompatibility of the alkaline electrolyte towards carbon dioxide is a major drawback. This is particularly true for a mobile application in which methanol is the favoured fuel [1–4], converted preferably by an on-board steam reforming yielding a CO_2-containing hydrogen gas.

Furthermore, the working temperature of the present alkaline fuel cells is restricted to ~80 °C since activated carbon, ordinarily used as a catalyst-support material, cathodically may not withstand higher temperatures [5]. This causes some difficulties with respect to water management and to waste-heat utilization, hence lowering the overall system efficiency.

In the 1960s, a low-pressure alkaline fuel cell with an internal methanol steam reforming has been developed [6, 7] solving some of the above-mentioned problems. The main idea was to separate the carbon dioxide from the reformer gas by a Pd–Ag membrane. Palladium and palladium alloys, especially Pd–Ag alloys with a high palladium content, are known for selective hydrogen permeation by chemisorbing and dissolving hydrogen as atoms. A cell unit consisted of a catalyst bed which contacted such a hydrogen permeable, nonporous $Pd_{75}Ag_{25}$ membrane anode [8] (Fig. 1) and a nickel-based cathode (Bacon type).

*New address: AFIF/Technopark, Pfingstweidstraße 30, 8005 Zürich, Switzerland.

0378-7753/93/$6.00

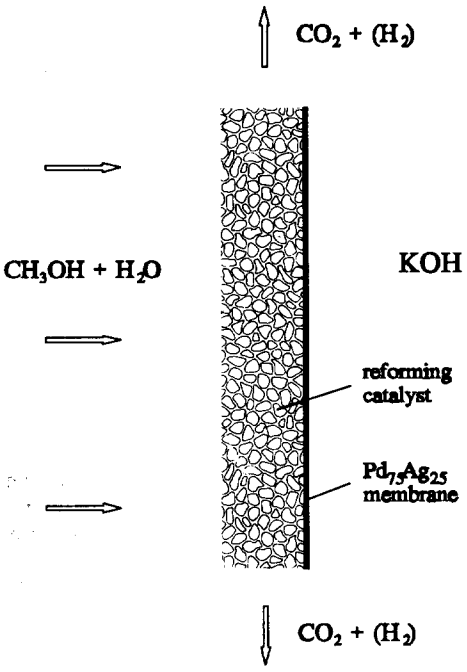

Fig. 1. Scheme of an internal methanol steam-reforming anode.

On the gas-side of the membrane anode, hydrogen from the methanol steam-reforming reaction:

$$CH_3OH + H_2O \overset{\text{cat.}}{\rightleftharpoons} CO_2 + 3H_2 \quad (1)$$

was selectively absorbed and, after diffusion through the membrane, electrochemically oxidized on the surface adjacent to the electrolyte. As a result of the continuous withdrawal of hydrogen, the equilibrium of the reforming reaction was shifted towards the reaction products and the temperature could be kept lower (200 °C) than in an ordinary methanol reformer. Spurious carbon monoxide was a minor problem [9] and system efficiency was high since waste-heat could be used directly for the evaporation of the methanol/water mixture and for the reforming reaction.

With this internal methanol reforming fuel cell operating with 85% KOH at 200 °C and a pressure of 1.7 bar (anode: CH_3OH:H_2O ratio is 1:1; 85% fuel utilization; cathode: air), current densities of 210 mA/cm^2 at 0.85 V were achieved with an energy conversion efficiency of 66% with respect to the lower heating value or 58% with respect to the higher heating value (without consideration of losses by auxilliary aggregates such as pumps). The main losses were caused by the cathode whereas the $Pd_{75}Ag_{25}$ anode had an overpotential of 30 mV only [6]. With an overpotential of 100 mV and pure hydrogen at 1.7 bar as fuel, an anodic current density of 1 A/cm^2 was obtained even at 150 °C [10] or of 700 mA/cm^2 at 120 °C [8]. However, the palladium-activated $Pd_{75}Ag_{25}$ membranes were 38 μm thick, requiring a prohibitive palladium amount of 35 mg/cm^2. Moreover, the concentrated caustic electrolyte revealed some corrosion and stability problems at elevated temperatures. Furthermore, the start-up

procedure was time-consuming because the fuel cell stack had to be preheated to the working temperature.

With this concept in mind, our goal was the development of an extremely thin Pd–Ag membrane applied on a porous metal screen. Equivalent anodic performance was desired but with a much less precious metal requirement and at a lower working temperature, thus reducing corrosion and stability problems and minimizing start-up time. In order to use waste-heat for the evaporation of the methanol/water mixture, the working temperature of the fuel cell must be above 100 °C for atmospheric pressure, preferably about 120 °C still allowing Teflon as a hydrophobic component for the cathodes. As cathodic catalysts, anorganic oxides such as lithiated Co_3O_4 [11] or pyrochlores, e.g. $Pb_2Ru_2O_{6.5}$ [12], may be taken into account. For such an 'intermediate temperature fuel cell' the reforming reaction must take place in a separate unit (external reforming).

Experimental

Preparation of the supported Pd–Ag membrane

The membrane anode was prepared by galvanic methods in a multistep process [13], which will be only briefly described (Fig. 2).

Since the deposition of poreless Pd–Ag layers is not on porous supports, a nonporous precursor material must be used which can be transformed into a porous structure after the deposition. Mainly due to its superior stability in caustic solution, nickel has been chosen as a support material, and a bimetallic foil proved to be useful as starting material*. For that purpose, initially a nickel-sieve structure with a thickness of ~50 μm was applied on a steel sheet by a photogalvanic process. After dissolution of the residual photoresist the holes were galvanically filled with copper (Fig. 2, step A).

The hexagonal holes had a diameter of 150 μm; the straps were 160 μm wide (Fig. 3) delivering a blank surface area of 23%**. Insufficient adhesion on the nickel-

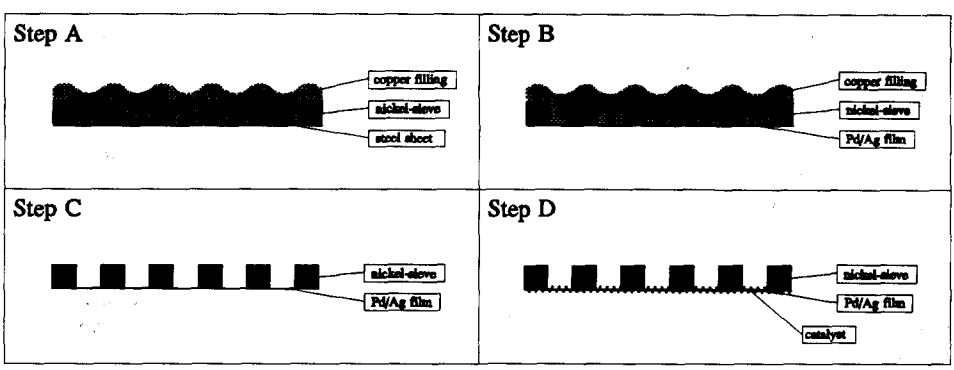

Fig. 2. Preparation of a nickel-sieve supported Pd–Ag membrane (schematic).

*As a first approach, selective demetallization of brass foil to leave a porous copper support [4] has been abandoned.

**A recently improved manufacturing process allows the deposition of straps less than 10 μm wide and with variable hole diameter, thus blank areas of more than 75% are possible.

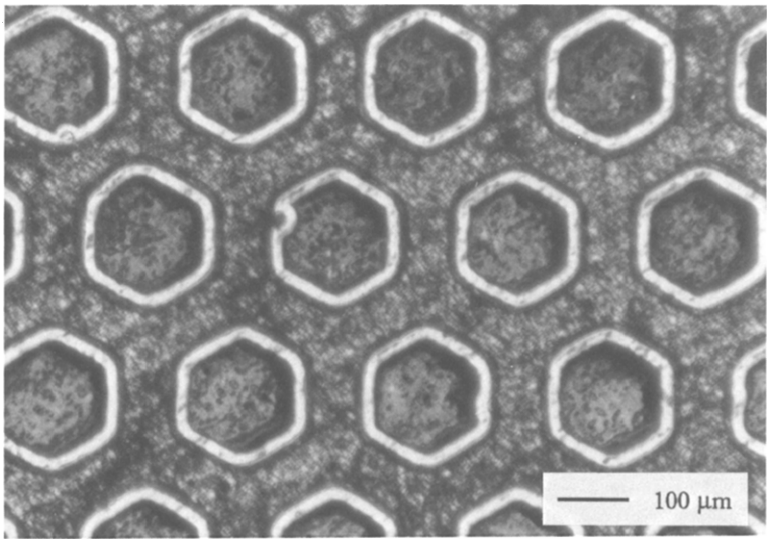

Fig. 3. Microscopic picture (polarized light) of a copper-plated nickel sieve.

sieve and sulfur impurities in the copper deposit were the main problems in the manufacturing of the bimetallic foils. So far, the maximum electrode diameter has been restricted to ~8 mm.

After removal of the bimetallic foil from the steel sheet, alloying was achieved at the contact area between copper and nickel by a thermal treatment in a reducing atmosphere (2 h at 700 °C in H_2). After further treatments (mechanical and electrolytical polishing) a thin Pd–Ag film was deposited unilaterally on the copper-plated nickel-sieve (Fig. 2, step B). The deposition of the Pd–Ag alloy was carried out potentiostatically at ±50 mV versus RHE (reversible hydrogen electrode) from a weakly alkaline electrolyte with glycine/glycinate as the major complexing agents. At limiting current and at low temperatures, poreless and uniform alloy deposits with almost no dendrites could be prepared with a thickness of <1 µm [14–16]. The composition of the alloy was $Pd_{73}Ag_{27}$. After this deposition, copper was selectively dissolved by anodizing for several hours in an alkaline tartrate electrolyte at 50 °C and at a potential of approximately +650 mV versus RHE (Fig. 2, step C). In order to prevent the destruction of the Pd–Ag film as a consequence of abrupt dehydrogenation, the applied potential had to be increased very carefully (1 mV/s) to the final value, starting from the open-circuit voltage. Finally a palladium-based catalyst layer was deposited on the Pd–Ag membrane (Fig. 2, step D). On each side, 1 mg palladium per cm^2 was deposited from an acidic electrolyte (50 mM $PdCl_2$, 1 M NaCl, pH 0.2) at room temperature. A maximum surface area of $A_{Pd,\,BET}=5.5$ m^2/g was obtained at +23 mV versus RHE [17]. Additionally, 0.01 mg Pt/cm^2 was deposited from an acidic electrolyte (3 mM $PtCl_4$, 2 M HCl) at 1 mA/cm^2 and at room temperature. Prior to the deposition of the catalytic layers, the membrane-supporting nickel screen was passivated in a weakly alkaline electrolyte at approximately +600 mV versus RHE for several hours. Due to this treatment, the adhesion of the catalytic layer on the nickel screen was weakened significantly, thus allowing its recovery.

Hydrogen-permeation measurements

The hydrogen-permeation experiments were carried out at different temperatures in a 100 ml Teflon vessel equipped with a magnetic stirrer (Fig. 4). Initially, the electrolyte was deaerated with nitrogen for 1 h. Since leaking at the edges of the anode mounting was a severe problem, the nickel-sieve supported Pd–Ag membrane had to be sealed to the PVDF (poly(vinylidene fluoride)) mounting with an epoxy resin (Araldit AV138 + HV998)*. The electrode surface area was therefore significantly reduced to ~ 0.09 cm^2, with an active surface area of 0.0185 cm^2. The latter was visually determined by counting the blank areas with a microscope. All measured current densities refer to this active surface area.

The supporting nickel sieve and the current collector were located on the gas-supply side. Hydrogen with a continuous flow rate of ~ 15 ml H_2/min was fed directly behind the anode and subsequently vented to the atmosphere through a thin Teflon tube. A platinum sheet (8 cm^2) was used as counter electrode, and a SCE (saturated calomel electrode, 25 °C; $E^0 = +241$ mV versus standard hydrogen electrode) with a 1 M KOH/10 M KOH salt bridge as reference electrode. The potential of the working electrode at zero current conditions was determined potentiodynamically as $ZCP_{70\ °C} = -1137$ mV versus SCE (ZCP = zero current potential) at 70 °C and ~ 1 bar H_2 by a potential–current plot (calculated value for the equilibrium potential at 25 °C: -1128 mV). The current values were determined by waiting for a constant current at each applied potential which typically required 2 min per data point.

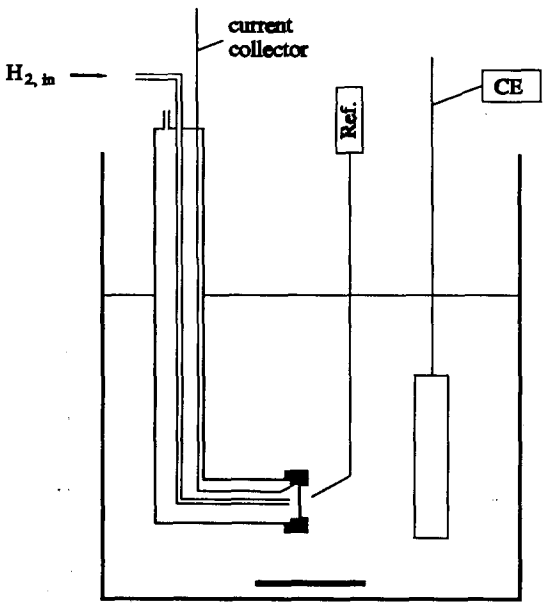

Fig. 4. Apparatus for the determination of hydrogen-permeation data for a nickel-sieve supported Pd–Ag membrane anode in alkaline solution. Ref.: SCE (saturated calomel reference electrode) and CE: platinum counter electrode.

*The chemical stability of the epoxy resin in 10 M KOH restricts the maximum operating temperature to about 110 °C.

The cyclic voltammograms were taken at a scan rate of 5 mV/s. Prior to the first cycle, a potential of −1150 mV versus SCE was applied for additional hydrogen loading during ~1 min.

The temperature dependence of the current was measured at −1110 mV versus SCE. Initially, the electrolyte was kept at 56 °C and the electrode was allowed to equilibrate for 10 min at the given potential. Then the temperature was raised with a rate of ~1 °C/min and data were taken at intervals of 5 to 10 °C.

The purity of the KOH was BioChemica MicroSelect (Fluka, Buchs, Switzerland). The water was ion-exchanged, refluxed in the presence of potassium permanganate and then bi-distilled.

Results and discussion

Hydrogenation of a $Pd_{73}Ag_{27}$ membrane at room temperature and ambient hydrogen pressure results in a remarkable volumetric expansion (Fig. 5). With nonactivated surfaces, the hydrogen in the Pd–Ag can be stored for several hours in the presence of air.

The lattice expansion of a $Pd_{75}Ag_{25}$ alloy, due to hydrogenation, is under these conditions 2.4% [18], corresponding to a volumetric dilatation of 7.5%. By increasing the silver content of the alloy up to 40 at.%, a reduction of the volumetric expansion of 3% can be achieved. However, both the hydrogen solubility [19] and especially the diffusion coefficient [20] decrease. Consequently, the maximum permeation rate is reduced considerably [21, 22].

Figure 6 shows two cyclic voltammograms of an activated Pd–Ag membrane anode in 10 M KOH at 70 °C and ambient hydrogen pressure. The first scan was started from a fully-hydrogenated membrane and exhibited much higher anodic currents than all the subsequent scans. These showed a characteristic peak current at approximately +25 mV versus $ZCP_{70\,°C}$. After four cycles, the shape and the size of the voltammograms remained constant.

The stationary potential–current density plot (Fig. 7), measured in 10 M KOH at 70 °C and ambient hydrogen pressure, shows an unusual behaviour. After a significant

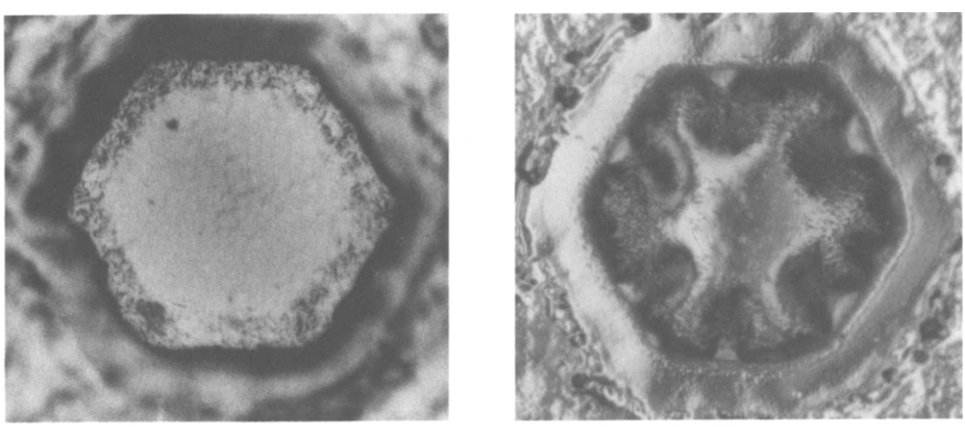

Fig. 5. Microscopic pictures (polarized light) of a (a) dehydrogenated and (b) hydrogenated $Pd_{73}Ag_{27}$ membrane (thickness: 0.7 µm; diameter of the blank field: 150 µm).

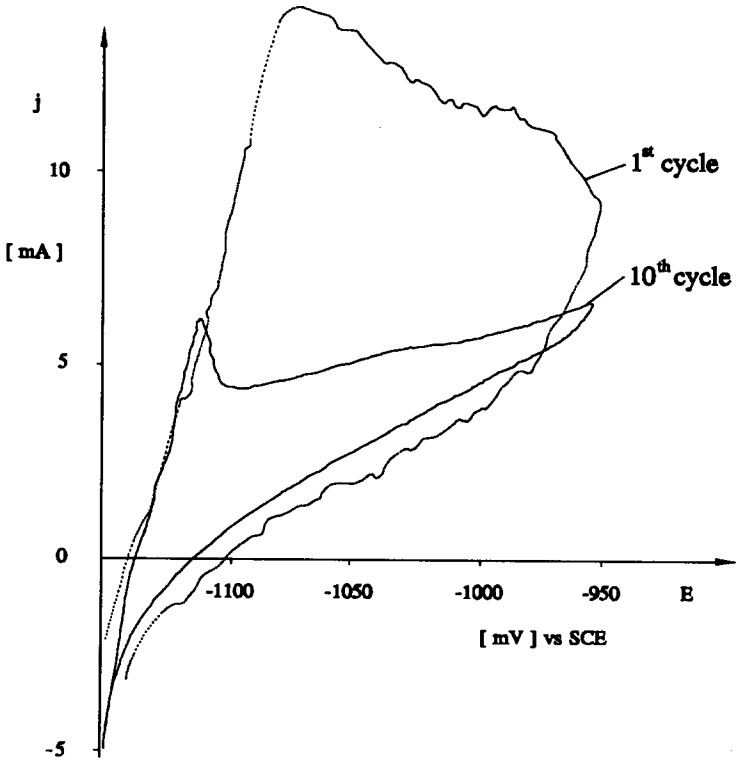

Fig. 6. Cyclic voltammograms at a nickel-sieve supported activated $Pd_{73}Ag_{27}$ membrane anode (thickness: 0.7 μm; catalyst: 1 mg Pd/cm^2 + 0.01 mg Pt/cm^2 on each side) in 10 M KOH at 70 °C and ambient hydrogen pressure; scan rate: 5 mV/s, scans starting at −1150 mV vs. SCE.

increase at small overpotentials the curve flattens and passes through a linear region before reaching the limiting current range ($j_{lim} = 360$ mA/cm^2). It is worth mentioning that the unexpected flattening occurs at the same potential as the peak current in the cyclic voltammogram.

Under the assumption of the validity of Fick's diffusion law:

$$j_{lim} = F\, D\, n_{H,in}/(v_{alloy}\, d)$$

(where $D\, n_{H\to 0} = 5.5 \times 10^{-7}$ cm^2/s [22], $v_{alloy} = 9.25$ cm^3/mole, $d = 0.7 \times 10^{-4}$ cm, and $F = 96\,500$ A s/mole); the hydrogen concentration at the entrance (gas side) can be calculated as $n_{H,in} = 0.004$ for the above-mentioned limiting current density. For equilibrium conditions, a hydrogen concentration of $n_{H,eq} = 0.36$ is possible [19] and thus would permit much higher permeation rates. Therefore, it can be assumed that solid-solution diffusion of hydrogen through palladium or Pd–Ag is not rate limiting*. Probably the hydrogen permeation is hindered at the interface between the Pd–Ag film and the palladium catalyst. Such an inhibition could be present on both sides of the Pd–Ag film.

*Unfortunately, those permeation rates cannot be calculated exactly since the diffusion coefficient generally is concentration dependent [23] and the validity of Fick's diffusion law is questionable in such a condition [24].

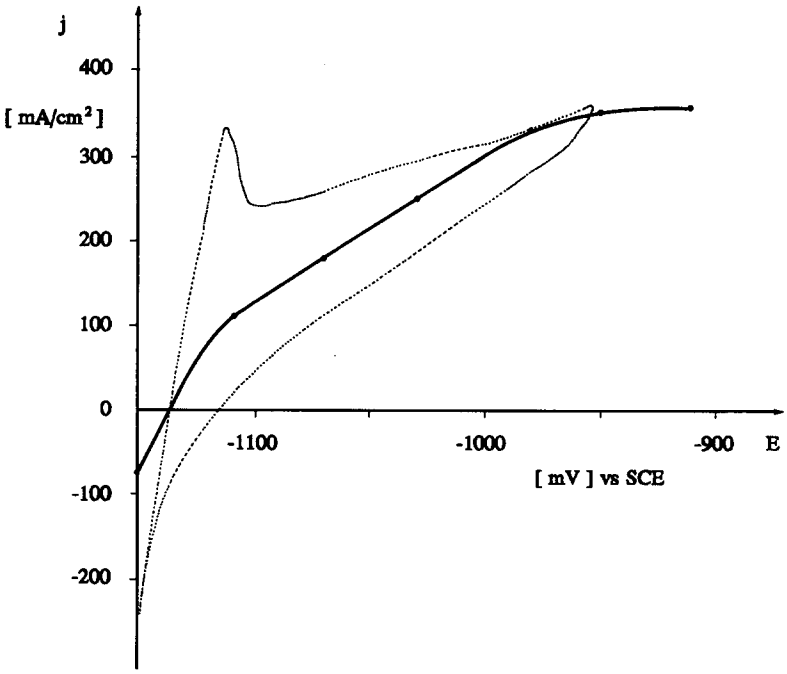

Fig. 7. Stationary potential–current density plot of a supported $Pd_{73}Ag_{27}$ membrane anode (thickness: 0.7 μm; catalyst: 1 mg Pd/cm² + 0.01 mg Pt/cm² on each side) in 10 M KOH at 70 °C and ambient hydrogen pressure; dotted line: cyclic voltammogram.

A further explanation for the reduced limiting current density may be given by a kinetic control of the hydrogen adsorption on the gas side of the membrane. On smooth (palladium) foils, surface diffusion of adsorbed hydrogen atoms between two different kinds of sites has been postulated as the rate-controlling step even at 200 °C by Wagner [25]. The model assumes that the dissociative hydrogen adsorption takes place at sites of type A and that the dissolution of adsorbed hydrogen into the metal takes place at other sites of type B. Surface diffusion of adsorbed hydrogen becomes rate determining when the reactions at sites of types A and B are both in equilibrium. The number of type A sites can be increased by using a catalyst whereas the number of type B sites can be enlarged, e.g., by mechanical deformation [26]. Thus, by shortening the average distance between the sites, the influence of surface diffusion will be substantially reduced. As a consequence, the dissociative adsorption rate can become rate determining, at least at low hydrogen partial pressures [27].

On the other hand, the dehydrogenation of palladium is known to be faster in the presence of reactive gases such as oxygen or ethylene than in vacuum or an inert gas atmosphere [28]. Therefore the desorption rate is favoured. The same may be true for the electrolytical oxidation of hydrogen. However, both the peak current observed in the cyclic voltammogram (Fig. 6) and the flattening of the potential–current curve at low overpotential (Fig. 7) are rather delicate to explain. The peak current cannot be attributed to dissolved hydrogen in the electrolyte as it has been done, e.g., for dispersed palladium black in 0.5 M sulfuric acid [29]. Despite the much lower hydrogen solubility in potash lye [30], the peak current density observed here is more

than 200 times larger than the peak current density of dissolved hydrogen in sulfuric acid.

A possible explanation for the unusual anodic behaviour could be found in the surface-activating platinum layer on the electrolyte side of the palladinated Pd–Ag membrane. Whereas in palladium (and in Pd–Ag) bulk diffusion of hydrogen is possible, platinum only allows surface diffusion due to its very low hydrogen solubility. At low current densities, the anodic oxidation of hydrogen occurs at the more active platinum sites, the hydrogen being supplied by bulk diffusion in the palladium and the subsequent surface diffusion on the platinum ('spillover'). Within this region, the potential–current curve is steep and the cyclic voltammogram exhibits a peak current. On enlarging the overpotential and thus the current density, at a certain point the surface-diffusion rate on the platinum becomes insufficient and the anodic hydrogen oxidation occurs mainly at the less active palladium sites yielding a flattened potential–current curve.

In a final experiment the temperature dependence of the current density at −1110 mV versus SCE (+27 mV versus $ZCP_{70\,°C}$) has been investigated in 10 M KOH and at ambient hydrogen pressure (Fig. 8).

It is noteworthy that an almost linear relationship is observed. By extrapolation to higher temperatures, at +27 mV versus $ZCP_{70\,°C}$ current densities of 350 mA per cm^2 blank surface (120 °C) and — more speculatively — 480 mA/cm^2 (150 °C) seem attainable.

To compare our results with literature data, another extrapolation may be made. Since the current density shows a linear behaviour with respect to the temperature (at +27 mV versus $ZCP_{70\,°C}$) as well as to the potential (at 70 °C, $+20\ mV < E < +150$ mV), a current density of 740 mA/cm^2 can roughly be calculated for 120 °C, +100 mV and ambient hydrogen pressure. For an optimized nickel-sieve structure with a 70% portion of blank area, an effective current density of 520 mA/cm^2 may be expected. This is 180 mA/cm^2 less than for $Pd_{75}Ag_{25}$ foils (38 μm thick) at a hydrogen pressure of 1.7 atm [8]. However, in our case the hydrogen pressure was lower, and only 2.5 mg of precious metal per cm^2 of apparent electrode surface area were needed instead of 35 mg/cm^2.

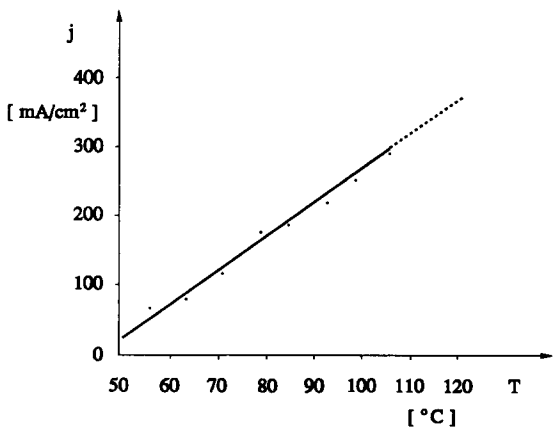

Fig. 8. Temperature vs. current density, at −1110 mV vs. SCE and ambient hydrogen pressure in 10 M KOH for a nickel-sieve supported activated $Pd_{73}Ag_{27}$ membrane anode (thickness: 0.7 μm; catalyst: 1 mg Pd/cm^2 + 0.01 mg Pt/cm^2 on each side).

Conclusions

Although the electrode tested is not yet optimized, the present results show that absolutely poreless Pd–Ag alloys with less than 1 μm thickness can be deposited as films on nickel-sieve structures. Furthermore, activated membranes can operate as hydrogen-permeation membranes with high current densities at low overpotentials in a strongly alkaline electrolyte. However, improvements have to be achieved in order to manufacture much larger electrodes exhibiting a 70% portion of blank surface area. In addition, it seems possible to improve and simplify the manufacturing process especially with respect to the surface activation.

The comparison of cyclic voltammograms with the stationary potential–current plot suggests that the hydrogen-permeation rate through such a membrane anode is mainly determined by gas-side reactions and/or by the hindered transition at the interfaces between the catalytic palladium layers and the Pd–Ag film. On the electrolyte side, surface diffusion on the additionally-deposited platinum seems to be important. With respect to the use of methanol steam-reformed fuel gas, a more detailed study of the rate-limiting steps will be necessary, particularly in the presence of carbon dioxide and of spurious amounts of carbon monoxide. A further goal is the development of a carbon monoxide-tolerant hydrogen-permeation membrane with less than 2.5 mg Pd/cm^2 promising a current density of 1 A/cm^2 at overpotentials of maximal +100 mV versus RHE, 120 °C and ambient pressure in strongly alkaline electrolytes. An improved version of the supported Pd–Ag membrane has to be tested for hydrogen-purification processes in the gas phase applying a pressure difference. For this purpose, a mechanical stabilization of the supported membrane can be achieved by a compressed ceramic powder. Finally, durability tests will be necessary.

Acknowledgement

The authors wish to express their thanks to the Swiss Federal Office for Energy Management for the financial support, and to the firm Iten AG, Rudolfstetten, Switzerland, for the supplementary galvanic work.

References

1 O. Lindström and C. Sylwan, Methanol air fuel cell for vehicles, *Ext. Abstr., Meet. The Electrochemical Society, Boston, MA, USA, May 6–11, 1979,* Vol. 79-1, pp. 50–52.
2 H. Wendt and W. Jenseit, *DECHEMA Monogr., 109* (1986) 77–89.
3 A. J. Appleby and F. R. Foulkes, *Fuel Cell Handbook*, Van Nostrand Reinhold, New York, 1989, pp. 186–190.
4 Th. Allmendinger, Ph. Hasler and W. Richarz, *Chimia, 42* (1988) 190–194.
5 A. J. Appleby and F. R. Foulkes, *Fuel Cell Handbook*, Van Nostrand Reinhold, New York, 1989, pp. 174, 370–376, 587–590.
6 A. J. Hartner and M. A. Vertes, *AIChE Symp. Ser., 5* (1965) 12–15.
7 M. A. Vertes and A. J. Hartner, *2e Journ. int. d'études des piles à combustibles, SERAI, Brussels, Belgium, 1965*, pp. 63–67.
8 H. G. Oswin and S. M. Chodosh, *Adv. Chem. Ser., 47* (1964) 61–72.
9 S. M. Chodosh, N. I. Palmer and H. G. Oswin, in B. S. Baker (ed.), *Hydrocarbon Fuel Cell Technology,* Academic Press, London, 1965, pp. 495–507.
10 S. M. Chodosh and H. G. Oswin, *2e Journ. int. d'études des piles à combustibles, SERAI, Brussels, Belgium, 1965*, pp. 109–115.

11 A. C. C. Tseung, D. B. Hibbert and N. P. Rasiyak, *US Patent No. 4 464 239 (1984).*
12 J. Singer and W. L. Fielder, *J. Power Sources, 29* (1990) 443–450.
13 Th. Allmendinger and Ph. Hasler, *Swiss Patent Applic. No. 00 737/92-6* (1992).
14 Th. Allmendinger and Ph. Hasler, *Int. Patent Appl. WO92/07 975* (1992).
15 Th. Allmendinger and Ph. Hasler, *Ext. Abstr., 42nd Meet. International Society Electrochemistry, Montreux, Switzerland, Aug. 1991*, Poster no. 5-57.
16 Ph. Hasler and Th. Allmendinger, *Surf. Coat. Technol.,* (1992) in press.
17 N. Ibl, G. Gut and M. Weber, *Electrochim. Acta, 18* (1973) 307–314.
18 S. D. Axelrod and A. C. Makrides, *J. Phys. Chem., 68* (1964) 2154–2159.
19 H. Brodowsky and E. Poeschel, *Z. Phys. Chem. Neue Folge, 44* (1965) 143–159.
20 A. Küssner, *Z. Phys. Chem. Neue Folge, 36* (1963) 383–386.
21 G. J. Bohmholdt, *Thesis*, University of Münster, Germany, 1966.
22 G. L. Holleck, *J. Phys. Chem., 74* (1970) 503–511.
23 A. Küssner, *Z. Naturforsch. Teil A, 21* (1966) 515–525.
24 Ph. Hasler, *Internal Rep. ENET 8 900 661/1* (microfiche), ETH Zürich, Switzerland, Oct. 1989.
25 C. Wagner, Z. Elektrochem., 44 (1938) 507–512.
26 A. Küssner, *Ber. Bunsenges. Phys. Chem., 66* (1962) 675–678.
27 W. Auer and H. J. Grabke, *Ber. Bunsenges. Phys. Chem., 78* (1974) 58–67.
28 E. Wicke and K. Meyer, *Z. Phys. Chem. Neue Folge, 64* (1969) 225–236.
29 T. Mallat and J. Petro, *Acta Chim. Acad. Sci. Hung., 112* (1983) 173–181.
30 C. L. Young (ed.), *IUPAC, Solubility Data Series,* Pergamon, Oxford, Vol. 5/6, 1981, pp. 40, 78.